

Solar Activity Effects on Propagation at 15 MHz
Received at Anchorage, Alaska USA on 10 September 2017

Whitham D. Reeve

1. Introduction

Solar cycle 24 continued its downward trend throughout 2017 but a surge in the Sun's activity occurred in the autumn. This paper discusses solar flare effects on 15 MHz time signal propagation to my Anchorage observatory on 10 September 2017. I previously reported on a Type II solar radio sweep that occurred on 20 October and was observed at my Coho Radio Observatory {[Reeve18](#)}. Some Type I radio noise storms also occurred during the autumn and I will report my observations of them in the near future. All times and dates in this paper are in Coordinated Universal Time (UTC) unless indicated otherwise.

Note: Internet links and references in braces { } parentheses () are provided in **section 8**.

2. Solar Active Region 2673

Solar active region 2673 was responsible for the effects discussed here. It produced a powerful X8.2 x-ray flare (figure 1) followed by a radio blackout on the propagation path between a 15 MHz time signal station and Anchorage, Alaska. Active regions contain one or more sunspots and are numbered consecutively by the US National Oceanic and Atmospheric Administration (NOAA). From mid-2002 on, sunspots numbers are truncated to four digits for reporting convenience, so the region in question is officially AR 12673. This active region alone produced four X-class and twenty-seven M-class flares between 1 and 10 September before it rotated around the Sun's west limb and out of view of Earth. For a description of x-ray flare magnitude classes see {[Flares](#)}.

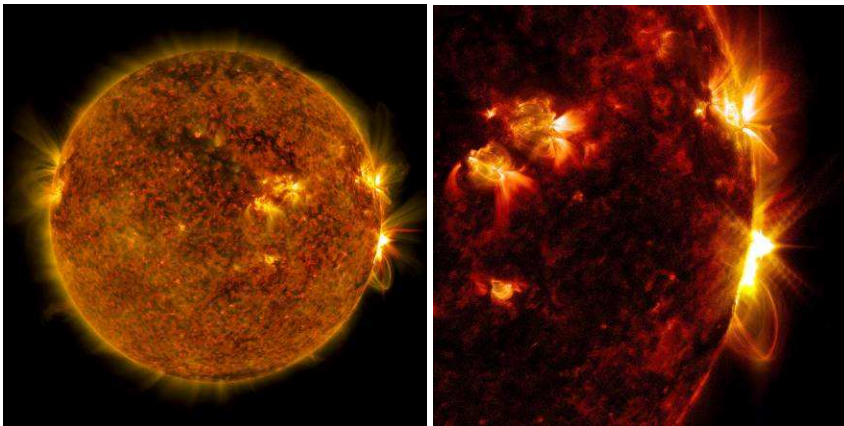


Figure 1 ~ **Left:** An X8.2 class solar flare in active region 2673 explodes 10 September 2017 on the edge of the Sun at the 3:00 position. This image was captured by NASA's Solar Dynamics Observatory (SDO) and is a composite of images at 171 and 304 Å wavelengths. **Right:** Close-up of the flare region is a composite of 171 and 335 Å wavelengths. Source: NASA/GSFC/SDO, {[NASA](#)}

Space Weather Prediction Center (SWPC) reported a coronal mass ejection with the flare. However, unlike a flare, which emits electromagnetic radiation in all directions at the speed of light, a CME contains charged particles (electrons and protons) from the Sun's corona, is directional and travels much slower. If the CME or part of it is Earth-directed it may disturb Earth's magnetosphere depending on the polarity of the CME's embedded magnetic field and other factors. In this case, the CME caused a geomagnetic storm a couple days after the flare. Further discussion of the CME is beyond the scope of this paper.

3. Solar Events during Time of Study

SWPC continually tabulates Individual solar events including those occurring during the time of this study (table 2). The solar activity included the already mentioned X8.2 x-ray (XRA) flare event, a couple much weaker C-class flares (also XRA), numerous radio bursts (RBR) over a very wide frequency range (245 to 4995 MHz) and Type II, Type III and Type IV radio sweeps (RSP) also over a wide frequency range (25 to 180 MHz). Of particular relevance to terrestrial radio propagation is the powerful X-class flare event.

Table 2 ~ Solar Events during time of study on 10 September 2017. The *Particulars* column shows the following: Class for x-ray flares (XRA); received levels in solar flux units (sfu) for radio bursts (RBR); Type/Importance for radio sweeps (RSP). A key to all abbreviations is available at [{EventsRead}](#). Data source: SWPC Events Report [{EventsRpt}](#)

| #Event | Begin | Max | End | Obs | Q | Type | Loc/Frq | Particulars | Reg# |
|---------------|-------------|-------------|-------------|------------|----------|------------|-------------|--------------------|-------------|
| 9010 + | 1419 | 1423 | 1425 | G15 | 5 | XRA | 1-8A | C1.6 2.7E-04 | 2673 |
| 9010 | 1422 | 1422 | 1423 | SAG | G | RBR | 410 | 170 | |
| . | | | | | | | | | |
| 9020 + | 1521 | 1521 | 1521 | SAG | G | RBR | 410 | 260 | |
| . | | | | | | | | | |
| 9030 + | 1523 | 1526 | 1528 | G15 | 5 | XRA | 1-8A | C1.0 1.4E-04 | 2673 |
| . | | | | | | | | | |
| 9040 + | 1535 | 1606 | 1631 | G15 | 5 | XRA | 1-8A | X8.2 1.4E00 | 2673 |
| 9040 + | 1550 | 1554 | 1608 | SAG | G | RBR | 1415 | 2400 | CastelliU |
| 9040 + | 1550 | 1554 | 1706 | SAG | G | RBR | 2695 | 1900 | CastelliU |
| 9040 + | 1551 | 1601 | 1706 | SAG | G | RBR | 4995 | 2600 | CastelliU |
| 9040 + | 1552 | 1559 | 1706 | SAG | G | RBR | 8800 | 10000 | CastelliU |
| 9040 + | 1552 | 1558 | 1706 | SAG | G | RBR | 15400 | 21000 | CastelliU |
| 9040 | 1553 | 1555 | 1606 | SAG | G | RBR | 610 | 1100 | CastelliU |
| 9040 + | 1553 | //// | 1624 | SAG | C | RSP | 025-180 | IV/2 | |
| 9040 + | 1553 | 1558 | 1604 | SAG | G | RBR | 245 | 670 | CastelliU |
| 9040 + | 1554 | 1556 | 1607 | SAG | G | RBR | 410 | 910 | CastelliU |
| 9040 | 1554 | //// | 1604 | SAG | C | RSP | 025-180 | III/2 | |
| 9040 + | 1608 | //// | 1612 | SAG | C | RSP | 025-043 | II/1 928 | |

4. Instrumentation and Propagation Path Characteristics

An Icom R-75 general coverage receiver, Argo software and an 8-element log periodic dipole array antenna were the main components used to monitor 15 MHz. The receiver was set to lower sideband (LSB) mode with AGC Off and was tuned 1 kHz above the carrier frequency to produce a trace on Argo at 1 kHz. The antenna was pointed toward WWV in Colorado with a setting of 107° true azimuth during the observations. A general system block diagram shows the main as well as additional components and accessories used to obtain these observations (figure 2).

All data were obtained automatically with the instrumentation described above. The receiver and associated PC were unattended. However, no audio recording was made, so I was unable identify the actual station being received, WWV in Colorado or WWVH in Hawaii. The 15 MHz WWV and WWVH transmitters are both rated 10 kW output power. The WWV-15 transmitter is connected to an omni-directional 1/2-λ (1/2-wavelength) vertical antenna and the WWVH-15 transmitter is connected to a directional antenna consisting of two 1/2-λ phased array vertical dipoles. Additional information on these stations may be found at [{WWV+H}](#). The great circle distance between the WWV station and Anchorage observatory is about 3800 km and almost entirely over land (figure 3). The distance between WWVH and Anchorage is about 4400 km and entirely over water. Positional data is provided for both stations for reference (table 1).

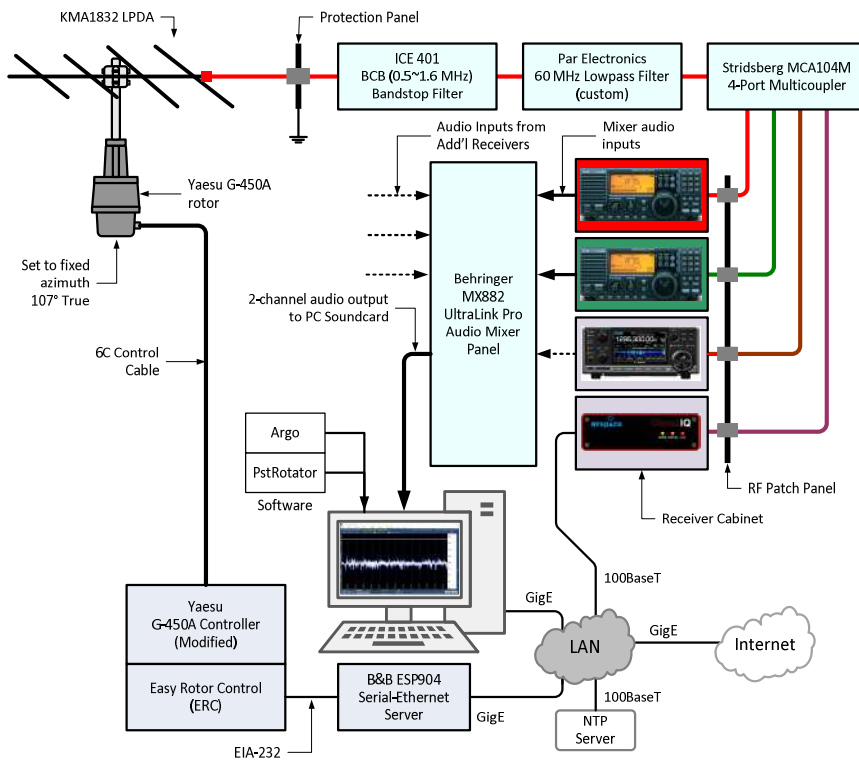


Figure 2 ~ General system block diagram for the Anchorage observatory:
Receiver: Icom R-75 general coverage receiver (red) fixed-tuned to 15 001 002 Hz (1 kHz offset with 2 Hz error from WWV at 15 MHz, LSB mode, AGC off)
Antenna: KMA Antennas KMA-1832, 8-element log periodic dipole array pointed at WWV (107° True azimuth)
Software: Argo, PstRotator
Soundcard: Realtek ALC223 chipset built into Lenovo ThinkCentre M900 Tiny desktop PC (stereo microphone input with all options and enhancements in the driver turned off). The PC runs 64-bit Windows 10 operating system. Not shown are support systems such as an ac uninterruptible power supply (UPS) and multi-voltage dc power supply. Image © 2018 W. Reeve

Figure 3 ~ Great circle maps for propagation between Fort Collins, Colorado (below, indicated as FNL) and Anchorage (ANC) and between Kauai, Hawaii (right, LIH) and Anchorage. Distances are about 3800 and 4400 km, respectively. Maps are from Great Circle Mapper {GCM}.

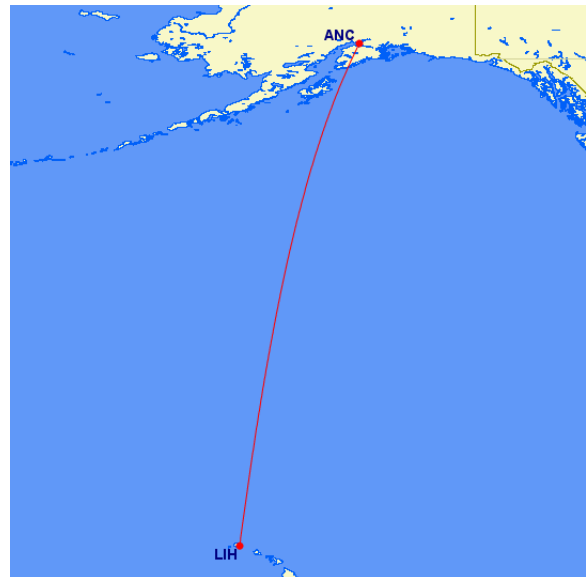
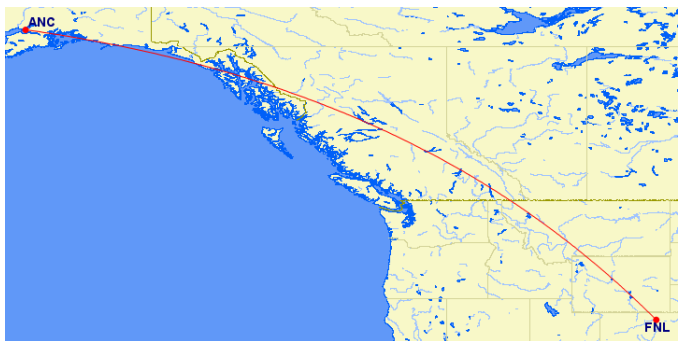


Table 1 ~ Station positions and propagation path endpoint details.

The solar elevations and azimuths are at 1606 UTC (time of X8.2 flare maximum). AMSL: Above Mean Sea Level

| Station | Geographical Coordinates | Station elevation (m AMSL) | Solar elevation (°) | Solar azimuth (°) |
|-----------|-----------------------------------|----------------------------|---------------------|-------------------|
| WWV-15 | 40° 40' 45.0" N, 105° 02' 24.5" W | 1582 | 37.5 | 121.5 |
| WWVH-15 | 21° 59' 15.3" N, 159° 45' 50.0" W | 3 | -5.1 | 82.8 |
| Anchorage | 61° 11' 58.0" N, 149° 57' 22.9" W | 20 | 5.2 | 89.8 |

For purposes of discussion I have assumed the transmitting station was WWV because propagation probably was not supported from WWVH up to the time of the solar flare and radio blackout. The results discussed below

do not depend on the origin station and I will refer only to WWV from here on. The radio propagation most likely consisted of multi-hop modes with refraction in the ionosphere's upper F-region. Assuming WWV and an F-region height of 250 km, the calculated elevation angles at the endpoints for propagation vary from 1.2° (1 hop) to 25.2° (4 hops); these calculations assume all hops use the same refraction height and the refraction regions are along the great circle path.

The previously-mentioned X8.2 flare occurred during the local morning at both stations. The sunrise time at WWV was 1236 UTC and morning nautical twilight lasted from 1136 until 1210. Sunrise at Anchorage was 1515 UTC and nautical twilight lasted from 1334 until 1430 (all solar position and time calculations from Multiyear Interactive Computer Almanac {MICA}). During nautical twilight the center of the Sun's disk is between 6° and 12° below the horizon. When the Sun is rising it starts to influence ionization above a given site during nautical twilight. However, it is the ionosphere along the path and not endpoints that determines the propagation. For reference, the time at a point midway between the sunrises at WWV and Anchorage was 1356 UTC. A solar terminator (gray line) map shows the terminator position at that time (figure 4).

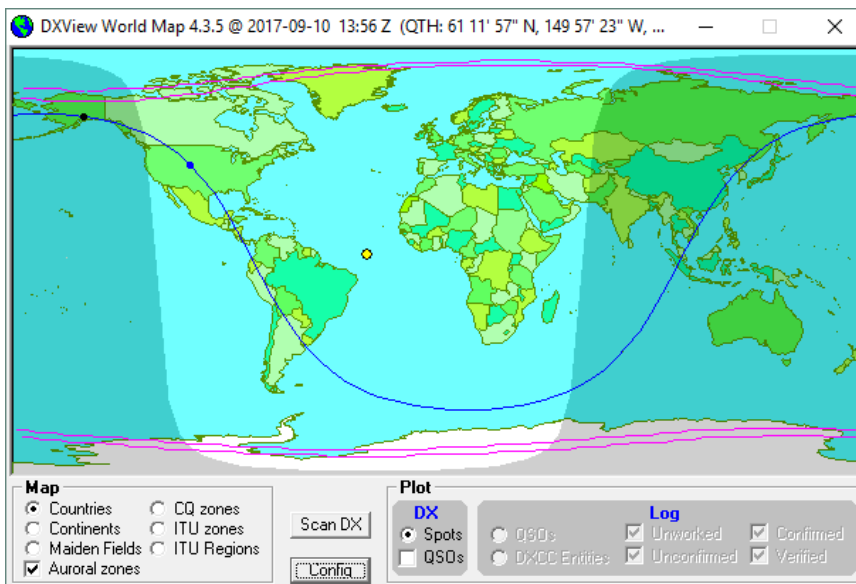


Figure 4 ~ Solar terminator map for 1356 UTC on 10 September 2017 showing the two endpoints, Anchorage and WWV (blue dots) and short and long propagation paths between them (blue line). The time of this plot is midway between the sunrises at the two stations and about 2 h before the solar flare. The Sun's position is marked by the small yellow circle between the coasts of South America and Africa, and the limits of the auroral oval are shown by magenta lines along the top and bottom of the map. Note that the Sun has not yet risen at WWVH in Hawaii. Image produced from DXView software {DXView}.

The International Reference Ionosphere, IRI-2016, is an ionosphere model available from Virtual Ionosphere, Thermosphere, Mesosphere Observatory {VITMO}. It can be used to estimate the ionosphere's conditions at any place on Earth and time after 1957. As a matter of curiosity I used the model to calculate the electron density with height at the midpoint on the WWV to Anchorage propagation path for 1356 UTC, corresponding to the solar terminator plot shown above, and F2-region height with time (figure 5). The reference ionosphere does not include any direct effects of the X8.2 solar flare or any transient solar activity.

The D-region is the lowest active layer in Earth's ionosphere, having an altitude of 60 to 90 km. The maximum electron density occurs at about 80 km and the half-thickness, where the electron density drops to one-half its maximum, is around 10 km (~80 ±5 km). The D-region appears after sunrise and attains maximum ionization when the Sun is at its highest position with respect to a given site. After that, the ionization in the region gradually decreases as electrons and ions recombine. The region is completely neutralized and disappears after sunset. The concentration of ions in the D-region during the day generally is not sufficient to reflect or refract HF radio waves. However, these waves are severely attenuated when they enter the D-region on both their upward and downward propagation paths to the F-region where refraction can take place.

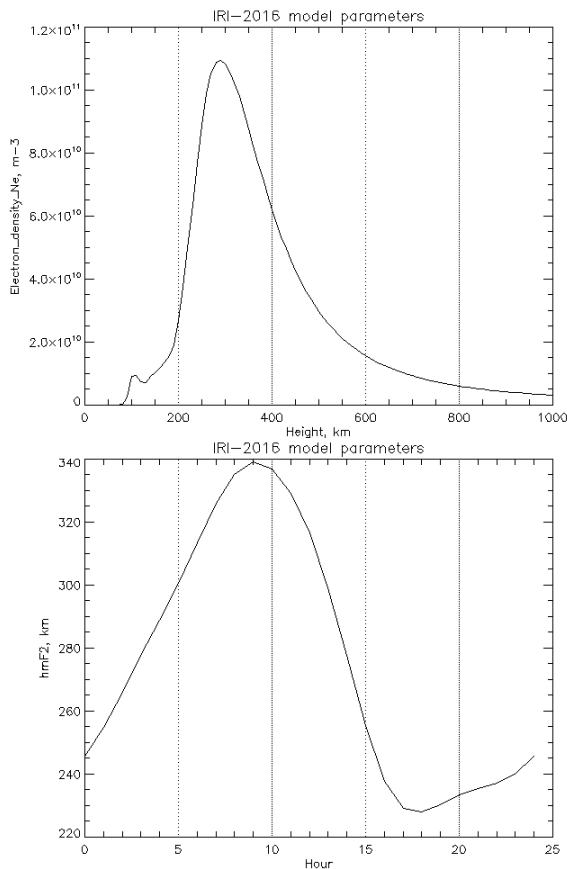


Figure 5 ~ IRI-2016 ionosphere model results for 10 September 2017 at geographic coordinates $50^{\circ} 56' 21.5''$ N, $127^{\circ} 29' 53.9''$ W, corresponding to the propagation path midpoint. It is important to note that the plots do not include flare effects and do not represent a model of the ionosphere at any other point along the path. Images source: {VITMO}

Upper: Plot of electron density ($Ne\ m^{-3}$) on the vertical scale and height (km) on the horizontal scale at 1356 UTC when propagation is first detected at Anchorage. Two points are of interest: 1) The electron density peak at about 280 km (slightly higher than the 250 km example used in the text), which represents the peak height of the ionosphere's F2-region and a likely refraction height for multi-hop propagation; 2) The electron density peak at about 110 km, which represents the modeled peak height of the ionosphere's E-region. The peak electron density in the D-region was about 30 km lower.

Lower: Plot of the modeled F2-region height (km) on the vertical scale and hour of day on the horizontal scale. The 280 km height at for 13.93 h (1356 UTC) corresponds to the time of the upper plot. The solar flare occurred between 1535 and 1631, when the F2-region would have been about 60 km lower than when propagation between WWV-15 and Anchorage was first detected.

The x-rays from a strong solar flare penetrate Earth's upper atmosphere as far as the D-region where they cause such intense ionization that practically all radio waves entering the region are absorbed. This phenomenon is called a *radio blackout* but it also has been called the *Mögel-Dellinger effect* [Siemens86], *shortwave fade* and *sudden ionospheric disturbance*. Radio blackout is the preferred usage in space weather reports when HF propagation is involved. A radio blackout can last from a few minutes to an hour or longer depending on the flare duration. The predicted D-region response to the X8.2 solar flare is discussed in section 6. At the same time that the D-region ionization is increasing in response to a flare, the critical frequency of the upper F-region (f_oF_2) is reduced, which in addition to D-region absorption, can further interrupt HF transmissions depending on their frequency.

5. Description of Received Signal

The solar effects on 15 MHz signal reception at Anchorage of the WWV time signal are shown by a sequence of images (figures 4.1 through 4.24). The entire sequence spans approximately 5 h, starting at 1354 UTC (0554 local Anchorage time) and ending at 1842 (1042 local).

The chart sequence is read left-to-right, top-to-bottom. Time is shown on the horizontal scale along the bottom of each chart image. Each chart spans about 12 min and each major (time-stamped) tick mark is 1 min. There is about 1 minute overlap between the images. Frequency is shown on the vertical scale along the right side. The frequency scale spans about 40 Hz from 980 to 1020 Hz and each major tick mark is 5 Hz. The receiver's sideband offset is 1000 Hz so the trace centered at 1000 Hz is the demodulated carrier. The setup shown uses 91.55 mHz FFT bin size (equivalent to resolution bandwidth). An unrelated trace is visible at the top of each chart but its source is unknown (probably a receiver artifact).

Prior to the beginning of the first chart at 1354, the ionosphere did not support propagation at 15 MHz between WWV and Anchorage. A couple minutes later at 1356 weak propagation is indicated by a faint trace at 1000 Hz. It is interesting to note that this time is exactly midway between the sunrise times at WWV and Anchorage and would correspond to sunrise at mid-path. Better propagation is established about four minutes later. Frequency deviations of ± 5 Hz occur as normal radiation from the rising Sun ionizes and reconfigures the upper atmosphere along the path. These frequency deviations are similar to sudden frequency deviations (SFD) caused by solar flares; see {Reeve15-1} and {Reeve15-2}.

The frequency deviations increase, reaching peak values of ± 10 Hz and continuing for over one hour when propagation starts to weaken along the path at about 1553. Only a few more minutes are needed before propagation ceases completely – the radio blackout. The X8.2 x-ray flare occurred at 1535, but it did not cause the radio blackout on the WWV to Anchorage path until about 20 min later. Peak x-ray flux was recorded at 1606, and the flare lasted almost one hour until 1631 according to the SWPC Events Report previously mentioned. Anchorage sunrise was at 1517 and had no obvious affects.

Radio blackout recovery starts at 1635, 4 min after the end of the flare at 1631. Recovery is only partial until approximately 1700 but a few partial dropouts and residual effects lasting several minutes are indicated until at least 1749. Note that the received signal frequency is relatively stable after the flare compared to before the flare. Considering sunrise and the resulting ionosphere reconfiguration along the path, the stable received frequency may have been a normal response even if the flare had not occurred.

Examination of the 10 September magnetogram for Anchorage (not shown here) indicates no obvious flare effects; however, SWPC reported a magnetic crochet at 1600 on Sun-facing terrestrial magnetometers.

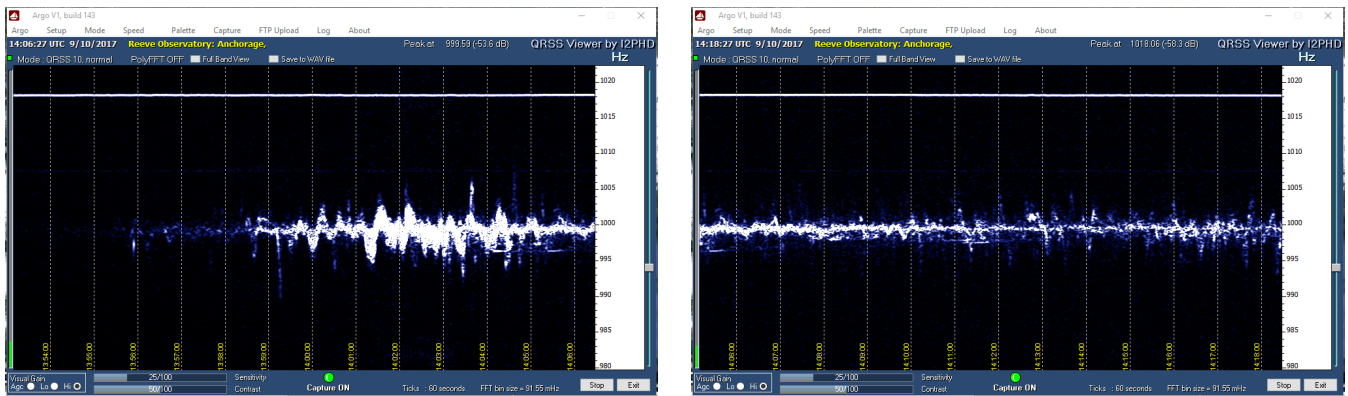


Figure 4.1 (left), 4.2 (right) ~ Start: 1354, End: 1418. Propagation to Anchorage start: 1357.

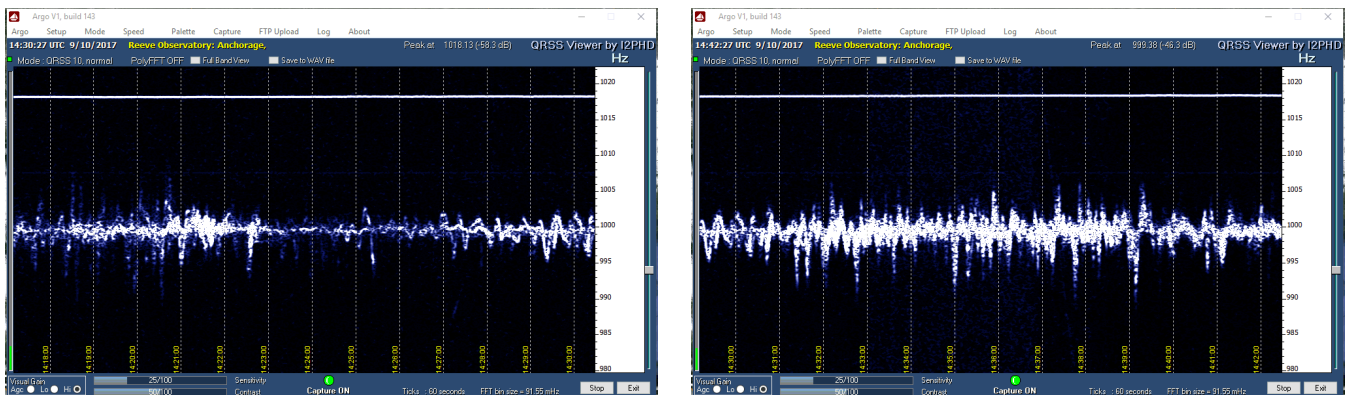


Figure 4.3 (left), 4.4 (right) ~ Start: 1418, End: 1442. WWV sunrise: 1439.

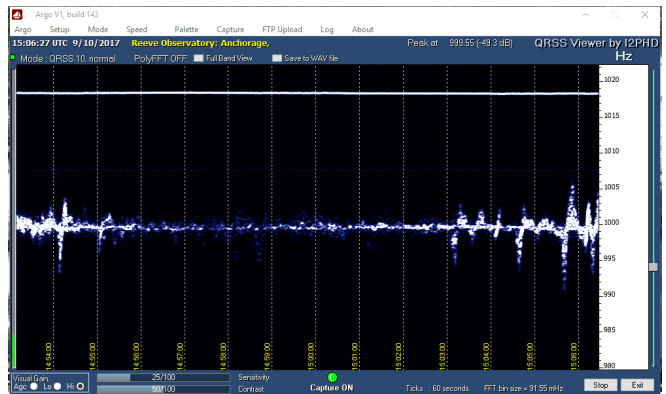
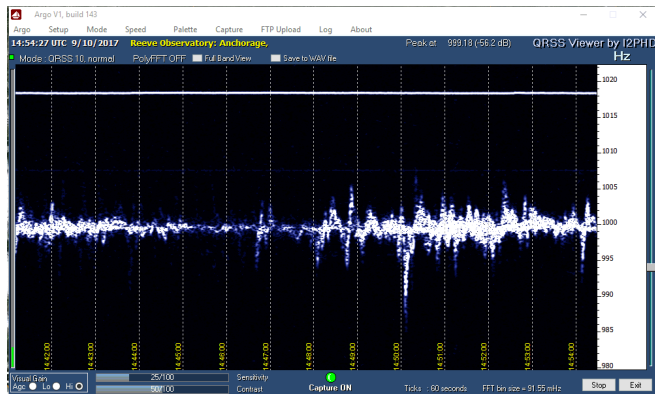


Figure 4.5 (left), 4.6 (right) ~ Start: 1442, End: 1506.

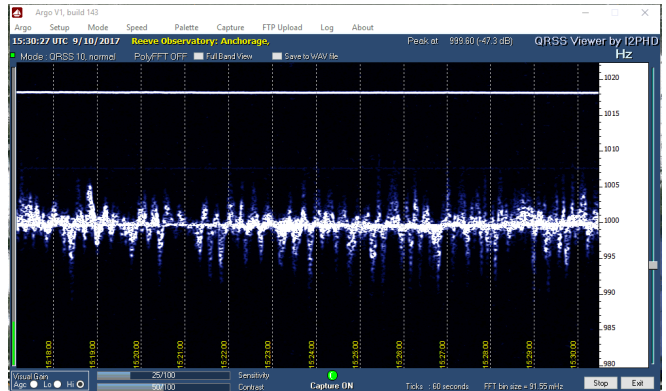
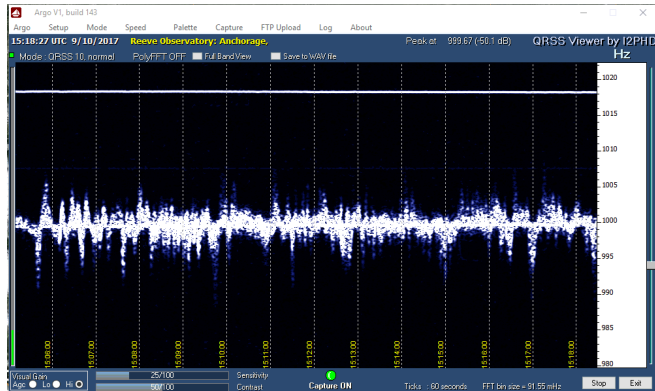


Figure 4.7 (left), 4.8 (right) ~ Start: 1506, End: 1530. Local sunrise: 1517.

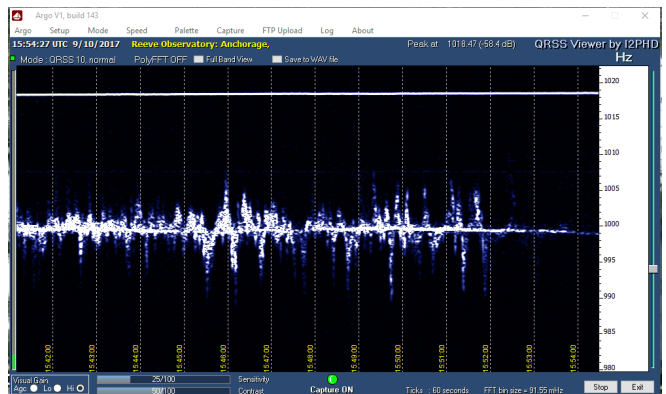
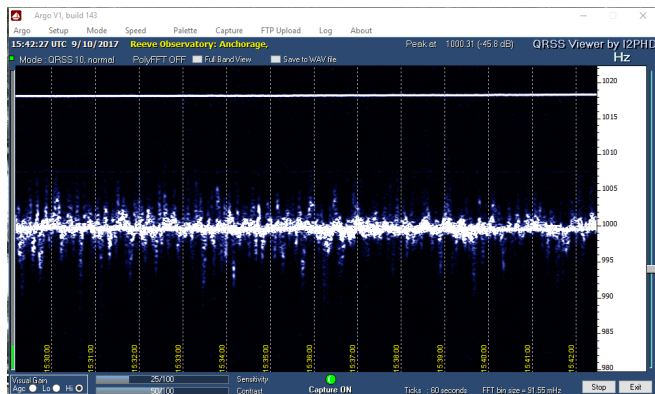


Figure 4.9 (left), 4.10 (right) ~ Start: 1530, End: 1554. X-ray flare start: 1535, Radio blackout start: ~1554.



Figure 4.11 (left), 4.12 (right) ~ Start: 1554, End: 1618. Radio blackout continues and is complete: ~1555.

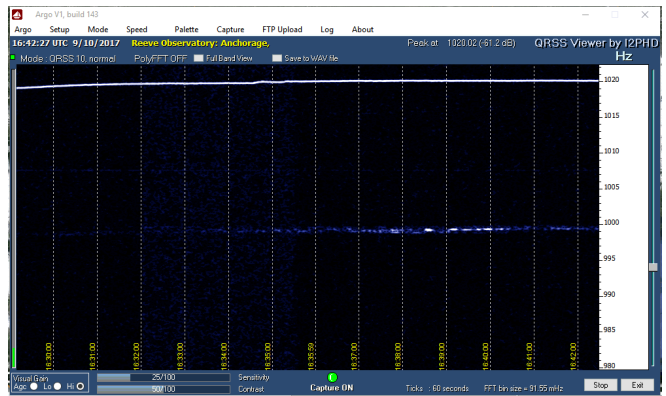
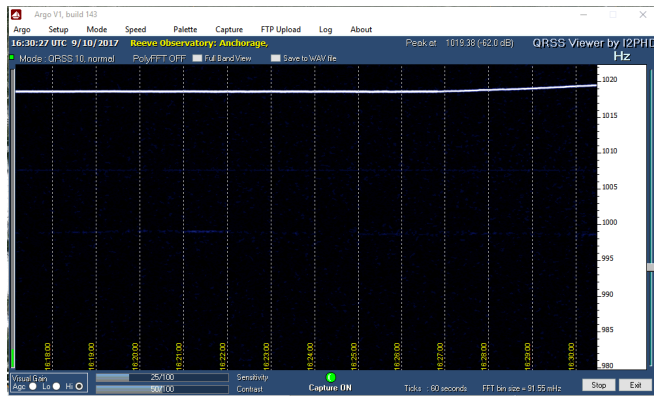


Figure 4.13 (left), 4.14 (right) ~ Start: 1618, End: 1642. X-Ray flare end: 1631, Radio blackout recovery start: ~1635.

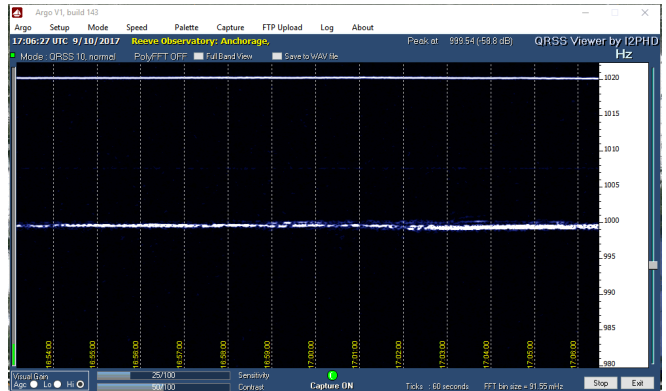


Figure 4.15 (left), 4.16 (right) ~ Start: 1642, End: 1706. Radio blackout recovery continues.



Figure 4.17 (left), 4.18 (right) ~ Start: 1706, End: 1730. Radio blackout end: ~1718, Residual propagation effects continue.

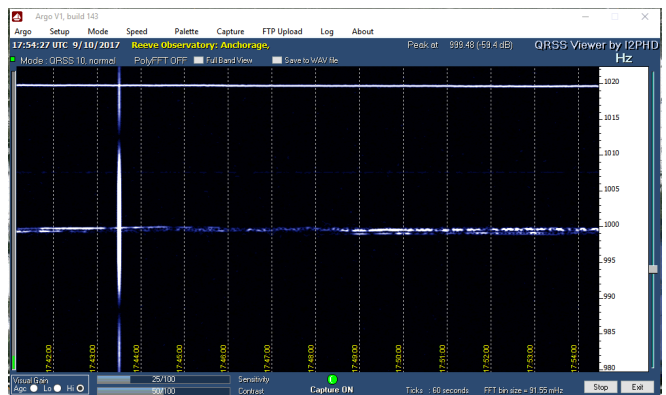
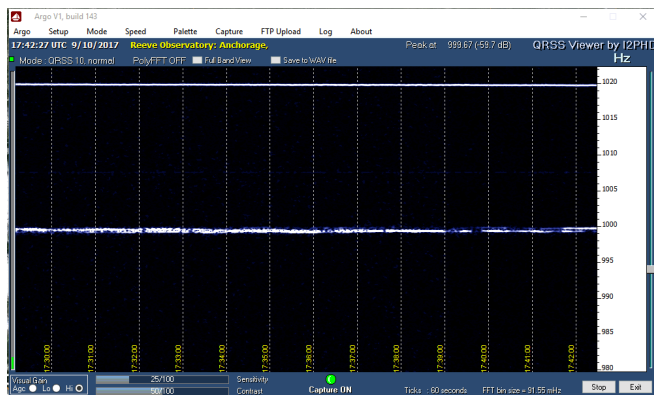


Figure 4.19 (left), 4.20 (right) ~ Start: 1730, End: 1754. Local coffee grinder RFI at 1743, Residual effects continue.

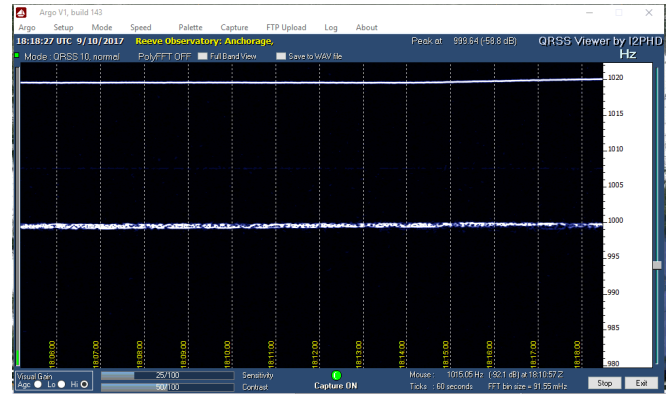


Figure 4.21 (left), 4.22 (right) ~ Start: 1754, End: 1818.

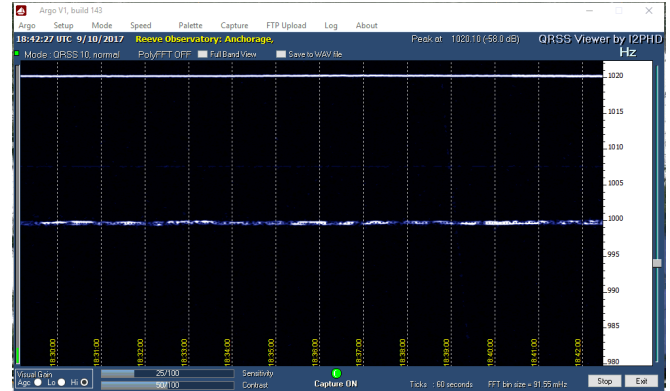
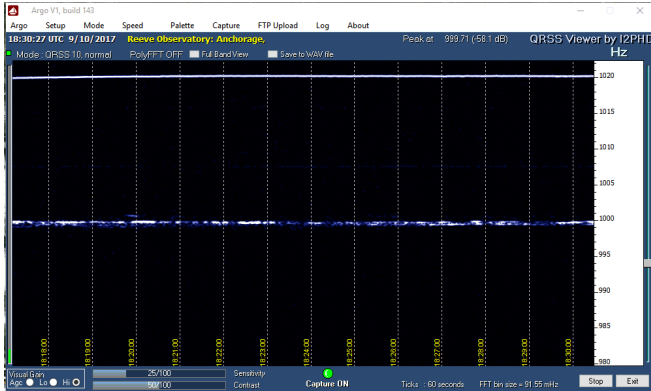


Figure 4.23 (left), 4.24 (right) ~ Start: 1818, End: 1842.

6. Predicted D-Region Response to the X8.2 Flare

Ionospheric absorption is depicted on D-Region Absorption Prediction (D-RAP) charts produced by SWPC. Three prediction charts are shown here, one for the onset of the radio blackout at 1554 (figure 5.1), one for the peak of the x-ray flare at 1606 (figure 5.2) and one for the start of recovery from the radio blackout at 1635 (figure 5.3). As previously mentioned, the recovery started only 4 min after the end of the flare. An explanation of the chart components is given after the figures.

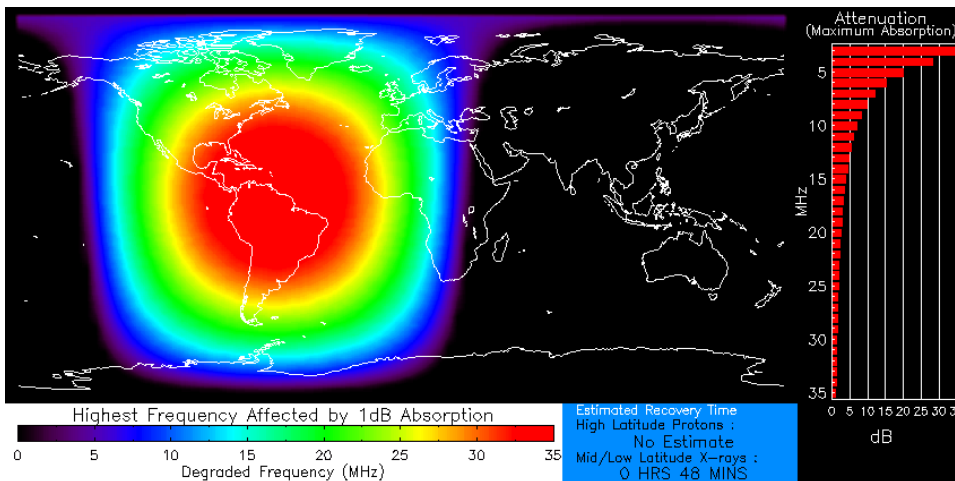


Figure 5.1 ~ D-RAP for 1554 UTC at onset of radio blackout at Anchorage, Alaska. The predicted absorption of a vertical incidence radio wave at 15 MHz is approximately 5 dB (from chart at right of main plot) but can be much higher for the long, oblique, multi-hop propagation path. See text. The predicted recovery time is 48 min (blue box). Image source: [{D-RAP}](#)

Moderate X-ray flux
Product Valid At : 2017-09-10 15:54 UTC

Normal Proton Background
NOAA/SWPC Boulder, CO USA

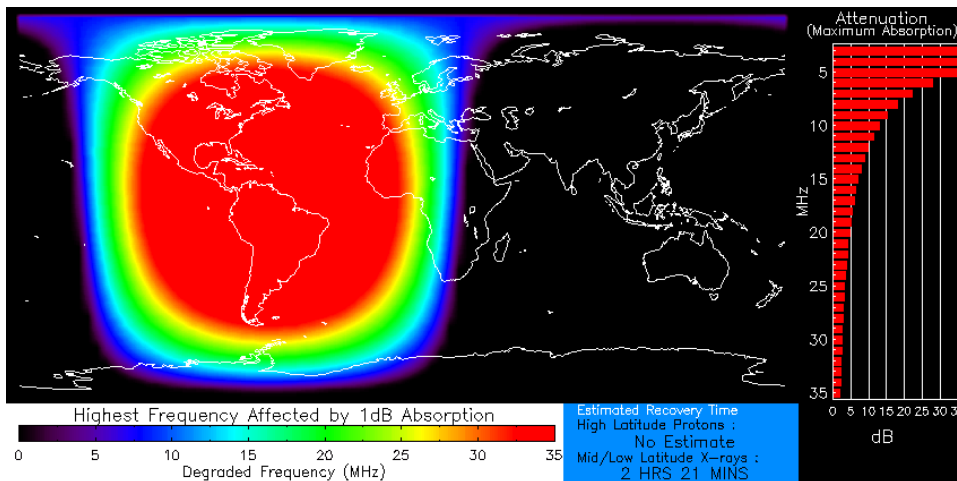


Figure 5.2 ~ D-RAP for 1606, the peak time for the X8.2 solar flare. The predicted absorption of a vertical incidence radio wave at 15 MHz is approximately 7.5 dB. The predicted recovery time is 2 h 21 min. Source: Same as above

Strong X-ray flux
Product Valid At : 2017-09-10 16:06 UTC

Normal Proton Background
NOAA/SWPC Boulder, CO USA

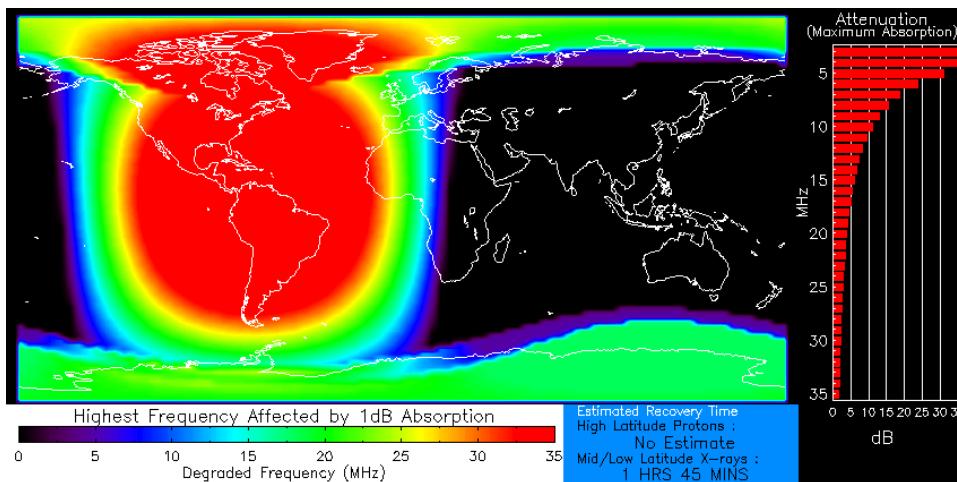


Figure 5.3 ~ D-RAP for 1635 at the start of radio blackout recovery. The predicted absorption of a vertical incidence radio wave at 15 MHz is approximately 6 dB. The predicted recovery time is 1 h 46 min. Source: Same as above.

Strong X-ray flux
Product Valid At : 2017-09-10 16:35 UTC

Normal Proton Background
NOAA/SWPC Boulder, CO USA

Key to D-RAP plots (adapted from {D-RAPDoc}):

Frequency map (main graphic display): The frequency map shows the predicted *Highest Affected Frequency* (HAF) as a function of latitude and longitude. HAF is the frequency that incurs 1 dB of loss (attenuation or signal degradation) during vertical propagation from the ground, through the ionosphere, and back to the ground. The degraded frequencies are indicated by color on the scale immediately below the main graph. The red area extends into the lower VHF band. It is important to note that radio frequencies lower than the HAF suffer an even greater loss than the 1 dB threshold. By definition, higher frequencies are unaffected. On a quiet day with no solar activity, the entire globe display is black.

Attenuation bar graph (right of the main graphic display): The bar graph shows the expected attenuation in dB as a function of frequency for vertical radio wave propagation at the point of maximum absorption on the globe (roughly above Venezuela during the times discussed here). The graph is valid only at that point, but it can be determined for any other location using the tabular data available with the D-RAP. The displayed bar graph values can be approximately scaled for oblique radio wave propagation by multiplying the bar graph values by $1/\sin(\alpha)$, where α is the elevation angle of the propagation path. Applying this to the low-angle propagation between WWV and Anchorage, the attenuation can be a factor of 8 to 50 times higher for each hop depending on the elevation angle or propagation mode (number of hops).

Estimated recovery time (blue box to right of frequency color scale): After an x-ray event (defined as flux greater than M1 levels) peaks and the flux begins to decrease, an estimated recovery time to normal (pre-flare)

background conditions is shown here. The estimate is based on empirically derived values relating the magnitude of a flare to the statistical average of the flare duration.

7. Conclusions

In this paper I provide background information and a series of received signal frequency plots that show how a strong solar flare can affect HF propagation. In particular, an X8.2 flare on 10 September from solar active region 2673 caused a radio blackout at 15 MHz on the propagation path between the WWV time signal transmitter in Colorado and a receiver in Anchorage in Alaska. The radio blackout, which lasted over 1 h, is put in the context of D-region absorption along that path as depicted on D-RAP plots obtained from SWPC. To monitor the transmissions, I used a general coverage receiver and software originally designed to detect very low speed CW transmissions. To study the propagation and radio blackout, I relied on online sources, such as Space Weather Prediction Center and others, for calculators, ionosphere absorption displays and solar events data.

8. References and Weblinks

- [Siemens86] Braun, G., Planning and Engineering of Shortwave Links, Siemens through John Wiley & Sons, 1986
- {D-RAP} https://www.ngdc.noaa.gov/stp/drap/data/2017/09/SWX_DRAP20_C_SWPC_20170910.zip
- {D-RAPDoc} <https://www.swpc.noaa.gov/content/global-d-region-absorption-prediction-documentation>
- {DXView} <http://www.dxlabsuite.com/>
- {Flares} <http://spaceweather.com/glossary/flareclasses.html>
- {GCM} <http://www.gcmapp.com/>
- {NASA} <https://svs.gsfc.nasa.gov/12706>
- {Reeve15-1} Reeve, W., Part I ~ Sudden Frequency Deviations Caused by Solar Flares, Concepts, published 2015, available at:
http://www.reeve.com/Documents/Articles%20Papers/Propagation%20Anomalies/Reeve_SuddenFreqDevConcepts_P1.pdf
- {Reeve15-2} Reeve, W., Part II ~ Sudden Frequency Deviations Caused by Solar Flares, Instrumentation and Observations, published 2015, available at:
http://www.reeve.com/Documents/Articles%20Papers/Propagation%20Anomalies/Reeve_SuddenFreqDevMeas_P2.pdf
- {Reeve18} Reeve, W., Type II Solar Radio Burst Observed on 20 October 2017, published 2018, available at:
http://www.reeve.com/Documents/CALLISTO/Reeve_TypeII-Burst.pdf
- {EventsRpt} <ftp://ftp.swpc.noaa.gov/pub/indices/events/20170910events.txt>
- {EventsRead} <ftp://ftp.swpc.noaa.gov/pub/indices/events/README>
- {MICA} <http://aa.usno.navy.mil/software/mica/micainfo.php>
- {SCTE} <http://www.stce.be/newsletter/pdf/2017/STCEnews20170915.pdf>
- {VITMO} https://omniweb.gsfc.nasa.gov/vitmo/iri2016_vitmo.html
- {WWV+H} <https://tf.nist.gov/general/pdf/1383.pdf>



Author: Whitham Reeve is a contributing editor for the SARA journal, Radio Astronomy. He obtained B.S. and M.S. degrees in Electrical Engineering at University of Alaska Fairbanks, USA. He worked as an engineer and engineering firm owner/operator in the airline and telecommunications industries for more than 40 years and now manufactures

electronic equipment used in radio astronomy. He has lived in Anchorage, Alaska his entire life. Email contact: whitreeve@gmail.com

Document Information

Author: Whitham D. Reeve

Copyright: ©2018 W. Reeve

Revisions: 0.0 (Original draft started, 10 Sep 2017)
0.1 (Major updates and additions, 10 May 2018)
0.2 (Added D-RAP images, 11 May 2018)
0.3 (Added positional data, 15 May 2018)
0.4 (Added SSN plot and ionosphere model plot, 18 May 2018)
0.5 (Updated sect. 3 to include WWVH, 11 Jun 2018)
0.6 (Minor updates to sect. 3, 22 Jun 2018)
0.7 (Relocated Solar Events, 28 Jun 2018)
0.8 (Minor edits and cleanup, 13 Jul 2018)

Word count: 3853

File size (bytes): 5669376